# The Chromatin Remodeler Protein CHD4 Cooperates With NKX2.2 to Regulate Pancreatic Beta Cell Integrity

Dylan K. Sarbaugh[1], Thais Gaia Oliveira[1], Michelle A. Guney[1], Victoria M. Hoelscher[1], Christopher J. Hill[1], Cole R. Michel[2], Kristen L. Wells[1], Richard K.P. Benninger[1], Lori Sussel[1]*

[1] Barbara Davis Center for Diabetes, University of Colorado Anschutz Medical Campus, Aurora, CO 80045
[2] School of Pharmacy, Mass Spectrometry Facility, University of Colorado Anschutz Medical Campus, Aurora, CO 80045

*Corresponding author: lori.sussel@cuanschutz.edu

## Abstract

NKX2.2 is a transcription factor that regulates pancreatic islet beta (β) cell identity and function; however, cofactor proteins that modulate the functional activity of NKX2.2 in β cells are relatively unexplored. An unbiased proteomics screen identified chromodomain helicase DNA-binding protein 4 (CHD4) as an NKX2.2 interacting partner. CHD4 is a nucleosome remodeler that directs the appropriate differentiation, maturation and function of many cell types by activating or repressing genes. To characterize the NKX2.2-dependent and independent roles of CHD4 in β cells, we generated *Chd4* βKO mice. Deletion of *Chd4* substantially impaired the maturation and function of β cells. The *Chd4* βKO mice were diabetic as early as 3 weeks of age due to the disruption of islet integrity, impaired glucose-stimulated insulin secretion and calcium signaling, and downregulation of essential β cell regulatory genes. These studies demonstrate that CHD4 is an essential transcriptional cofactor of NKX2.2 that is required for the proper maturation and function of pancreatic β cells.

## Introduction

Blood glucose homeostasis is maintained by the pancreatic islets of Langerhans. Adult pancreatic islets are comprised of four major hormone producing endocrine cell types including the beta (β) cells that secrete insulin to lower blood glucose levels and pancreatic alpha (α) cells that secrete glucagon to raise blood glucose levels. When pancreatic β cells become dysfunctional or destroyed, diabetes mellitus occurs, which is an increasingly prevalent disease worldwide. Understanding the transcriptional networks and proteins that maintain appropriate pancreatic β cell maturation and function are essential for understanding the pathophysiology of diabetes to facilitate improved treatment options and/or leading to a cure for diabetes.

The combinatorial temporal and spatial expression of transcription factors allows for appropriate cell differentiation, maturation, and function. In the pancreas, numerous studies over the past 30 years have identified many of the transcriptional regulatory pathways that regulate islet cell development and function (1-3). Each islet population initiates independent transcriptional programs, expressing a cohort of essential transcription factors that help establish its proper development, maturation, and functional identity.

NKX2.2 is an essential transcription factor required for the proper development, maturation and function of β cells in mice and humans. In *Nkx2.2* null mice, there is a complete absence of β cells, a severe reduction of α cells, and a substantial increase in ghrelin producing cells, leading to neonatal diabetes and death (4, 5). In humans, homozygous loss of function mutations in *Nkx2.2* also results in neonatal diabetes (6). To study the role of NKX2.2 specifically in β cells, *Nkx2.2* was deleted in developing and mature β cells (*Nkx2.2* βKO mice). These mice

survive into adulthood, however the mutant β cells were severely dysfunctional and a proportion of β cells either failed to produce insulin or lost their β cell identity and became polyhormonal (7).

NKX2.2 has 3 protein domains, the tinman (TN) domain, the homeodomain (HD) which binds DNA and the NK2 specific (SD) domain. To dissect which domains of NKX2.2 are important for β cell function, mouse models that deleted either the TN domain or the SD domain were generated (8, 9). Characterization of mice lacking the TN domain (*Nkx2.2*$^{TNMut}$), resulted in dysfunctional β cells that were either immature or transdifferentiated into α cells. Molecular experiments showed the NKX2.2 TN domain is required for the repressive activity of NKX2.2 by recruiting the Transducer-like enhancer of split 3 (TLE3)/Groucho-related gene 3 (GRG3) and Histone deacetylase 1 (HDAC1) to many repressed targets, including the master α cell regulator Aristaless homeobox gene *(Arx)* promoter (8). This study showed the importance of the TN domain as a major contributor to *Nkx2.2*'s role of repressing non-β cell genes in β cells.

Characterization of mice lacking the SD domain (*Nkx2.2*$^{SDMut}$) resulted in elevated blood glucose levels due to down regulation of β cell maturation and identity genes, among other phenotypes (9). It is still unknown what cofactor proteins the NKX2.2 SD domain interacts with to allow this activation role. These previous studies showed that NKX2.2 activates β cell genes and represses non-β cell genes; however, the mechanisms underlying these contrasting roles of NKX2.2 in the same cell type is currently unknown. To better characterize *Nkx2.2's* function in β cells it is necessary to identify the cofactor proteins NKX2.2 interacts with as well as the roles of those proteins themselves in the β cell.

In this study, we set out to uncover essential cofactor proteins of NKX2.2 and determine their role in β cells. We identified Chromodomain Helicase DNA-binding Protein 4 (CHD4) as a NKX2.2 interacting factor and generated mice that deleted *Chd4* specifically in the developing β cells. These studies demonstrated that CHD4 is important for the proper maturation and function of β cells and the structural integrity of islets. Furthermore, we uncovered both NKX2.2 dependent and independent roles for CHD4 during β cell maturation.

## Results

### *CHD4 and NuRD complex proteins interact with NKX2.2 in pancreatic β cells*

NKX2.2 has been shown to function as a repressor and activator in pancreatic islets (5, 7-9). To identify cofactors of NKX2.2 that may influence its function in pancreatic β cells, we performed an unbiased screen for interacting proteins. Mouse Insulinoma 6 (MIN6) β cells were transfected with *Nkx2.2*-encoding plasmids that incorporated 3 myc epitope tags at the N-terminus of the full-length NKX2.2 protein and several previously characterized *Nkx2.2* mutant derivatives (TN$^{mut}$, SD$^{mut}$, TN$^{mut}$/SD$^{mut}$) (8, 9) (Figure 1A). A myc-tagged empty vector (EV) was used as a control. This strategy not only allowed an unbiased identification of NKX2.2 cofactors but also potentially identified cofactors that were dependent on specific NKX2.2 protein domains. An anti-MYC antibody was used to immunoprecipitate (IP) the NKX2.2 proteins, followed by mass spectrometry (MS) analysis. The IP-MS with NKX2.2 wild type (WT) identified the most interacting proteins with 211 proteins enriched at least 2-fold in abundance compared to the EV control. From the NKX2.2 TN$^{mut}$ and NKX2.2 SD$^{mut}$ pulldowns, we identified 169 and 143 interacting proteins, respectively, that were enriched at least 2-fold in abundance compared to the EV control. Interestingly, from the NKX2.2 TN$^{mut}$/SD$^{mut}$ pulldown, we only identified approximately 84 interacting proteins, suggesting that deletion of the SD domain disrupted a substantial number of interactions, independently and in cooperation with the TN domain.

The IP-MS identified DNMT3A, DNMT1 and HDAC1, proteins that had been previously shown to interact with the NKX2.2 TN domain to repress the *Arx* locus in β cells (8, 10). In addition to identifying known interacting proteins, several members of the Nucleosome Remodeling and Deacetylase (NuRD) complex, including the functional enzymatic protein Chromodomain Helicase DNA-binding Protein 4 (CHD4) were identified in the screen (Figure

1B). CHD4 showed the highest enrichment in the NKX2.2 WT and the NKX2.2 $TN^{mut}$ samples and the interaction appeared to be weakened in the NKX2.2 $SD^{mut}$ and NKX2.2 $TN^{mut}/SD^{mut}$ samples. The interaction between the NKX2.2 domains and CHD4 was validated through Co-Immunoprecipitation (Co-IP) followed by Western blot (Figure 1C), which showed a similar pattern of enrichment observed in the IP-MS. The interaction between NKX2.2 and CHD4 was disrupted to a greater extent in the NKX2.2 $SD^{mut}$ and NKX2.2 $TN^{mut}/SD^{mut}$ samples, suggesting the SD region may be the main domain facilitating the interaction of NKX2.2 and CHD4.

Both the NuRD complex and CHD4 specifically have been implicated as necessary for proper development, maturation and function of many different tissues and cells, often acting as gene repressors by deacetylating histones and remodeling chromatin (11-15), although activation of genes has been noted as well (16, 17). To further validate an interaction between CHD4 and NKX2.2, we immunoprecipitated CHD4 from MIN6 nuclear lysate followed by MS. As expected, this identified the other NuRD complex components (HDAC1 and 2, MTA1, 2 and 3, RBBP 4 and 7, MBD 2 and 3), many of which were also present in the NKX2.2 WT MS. NKX2.2 was also identified in the CHD4 IP-MS. We further verified the interaction between CHD4 and NKX2.2 by pulling down CHD4 in MIN6 nuclear lysate and western blotting for endogenous NKX2.2 (Figure 1D).

Comparison between proteins that interacted with either NKX2.2 WT and CHD4 identified 112 proteins as cofactors of both NKX2.2 and CHD4. Greater than half of the significantly enriched protein cofactors identified in the NKX2.2 WT MS were also significant CHD4 protein cofactors and a hypergeometric test confirmed that this represents a statistically significant enrichment ($p < 0.001$). A String database (18) was used to group the 112 proteins using K means clustering into 3 main clusters (Supplementary Figure 1A). CHD4 and 32 other proteins were clustered as a protein group associated with heterochromatin. Interestingly, in addition to HDAC1 and HDAC2, DNMT3A and DNMT1 interacted with both CHD4 and NKX2.2 (Figure 1E). Due to the known repressor functions of DNA methyltransferases and histone deacetylases (19), we hypothesized that NKX2.2 recruits CHD4 to specific sites in the β cell genome to facilitate repression by closing chromatin and repressing non-β cell genes. To test this hypothesis, we investigated the role of CHD4 in mouse β cell development, maturation and function.

*Pancreas knock out of Chd4 leads to blood glucose and body weight defects*

*Chd4* is expressed in all pancreatic islet cells types (20) and has a role in regulating adult β cell function through an interaction with Pancreas Duodenum Homeobox1 (PDX1) (21, 22); however, its role in regulating islet development and maturation, where NKX2.2 plays a major role, had not yet been assessed. To determine whether CHD4 functions during pancreas development we generated mice carrying a *Chd4* floxed ($Chd4^{(fl/fl)}$) (16) allele and a $Pdx1^{(Cre/+)}$ (23) allele which would remove CHD4 from the entire pancreas and duodenum at the onset of pancreas formation (Supplementary Figure 1B). The $Chd4^{(fl/fl)}; Pdx1^{(Cre/+)}$ mice displayed a significant increase in the *ab libitum* blood glucose as early as postnatal day 2 (P2) and through 4 weeks of age compared to $Chd4^{(fl/fl)}$ and $Chd4^{(fl/+)}; Pdx1^{(Cre/+)}$ control mice (Supplementary Figure 1C). Morphometric analysis using immunofluorescent (IF) staining did not reveal an alteration of islet cell numbers or islet architecture at P2; but there was a severe disruption in islet structure at 4 weeks of age (Supplementary Figure 1D). However, there was also a significant decrease in body weight of mutant $Chd4^{(fl/fl)}; Pdx1^{(Cre/+)}$ mice compared to $Chd4^{(fl/fl)}$ and $Chd4^{(fl/+)}; Pdx1^{(Cre/+)}$ mice at P2 and 4 weeks of age (Supplementary Figure 1C). This suggests that removing *Chd4* from the pancreatic exocrine, ductal, and intestinal duodenal cells, in addition to loss of *Chd4* from the pancreatic endocrine lineage may disrupt the proper secretion of digestive enzymes and/or digestion of foods. Since assessment of endocrine pancreas function could be confounded

149 by the defects in these other tissues that caused significant body weight loss, we chose to focus on
150 the role of CHD4 specifically in the developing β cells.
151
152 *Chd4 βKO causes no overt developmental phenotype*
153 To characterize the function of CHD4 in developing β cells from the onset of their
154 differentiation, we generated *Chd4*$^{(fl/fl)}$; *Ins1*$^{(Cre/+)}$ (24) mice (hereafter referred to as *Chd4* βKO
155 mice). Deletion of the CHD4 protein specifically from the β cell lineage was confirmed through
156 Western blot analysis using mouse islet lysate (Supplementary Figure 2A). Because CHD4 is
157 present in other islet cell types, we further validated the β cell deletion using IF staining
158 (Supplementary Figure 2B). At all ages tested, deletion of *Chd4* from the β cells did not result in a
159 body weight phenotype (Supplemental Figure 2C). To characterize *Chd4* βKO mice, we
160 performed morphometric analysis and assessed blood glucose at postnatal day 2 (P2).
161 Unexpectedly, given the severe developmental phenotypes associated with deletion of *Pdx1* or
162 *Nkx2.2* in developing β cells (4, 5, 25-27), and the known interaction of PDX1 and NKX2.2 with
163 CHD4, the neonatal *Chd4* βKO mice had normal blood glucose levels (Figure 2A), as well as no
164 change in the hormone area of insulin, glucagon or somatostatin (Figure 2B), compared to control
165 mice. There were also no apparent alterations in the islet architecture or structure when comparing
166 *Chd4* βKO mouse islets to control mouse islets (Figure 2C), suggesting that CHD4 is not
167 necessary for specification or early development of the β cell lineage.
168
169 *Chd4 βKO mice are glucose intolerant by 3 weeks of age*
170 At 3 weeks of age, shortly after weaning, combined male and female *Chd4* βKO mice had
171 significantly higher fasting blood glucose levels (Figure 2D) when compared to control mice that
172 included *Chd4*$^{(fl/fl)}$, *Ins1*$^{(Cre/+)}$ (*Cre* only control) and *Chd4*$^{(fl/+)}$; *Ins1*$^{(Cre/+)}$ (Het) mice. Because
173 none of the control mice of any genotype displayed defects in fasting blood glucose levels or
174 glucose tolerance (Supplementary Figure 3), subsequent experiments included only *Chd4*$^{(fl/fl)}$
175 (control) and *Chd4*$^{(fl/fl)}$; *Ins1*$^{(Cre/+)}$ (*Chd4* βKO) mice. When assessing sex separately at 3 weeks,
176 only female *Chd4* βKO mice showed significantly higher fasting and *ad libitum* blood glucose
177 levels compared to controls and were glucose intolerant (Supplementary Figure 4A).
178 Morphometric analysis performed on combined male and female mice at 3 weeks of age showed a
179 significant decrease in the insulin positive hormone area, no change in the glucagon positive area,
180 and a slight but significant increase of the somatostatin positive hormone area in *Chd4* βKO
181 compared to control mice (Figure 2E). In addition to the changes in hormone expression area,
182 islet architecture was disrupted in *Chd4* βKO mice compared to control mice; glucagon and
183 somatostatin expressing cells, typically present at the periphery of the islet, were present in the
184 islet core where only β cells are normally seen (Figure 2F). Interestingly, we did not observe the
185 formation of polyhormonal cells, as was seen in the Nkx2.2 βKO mice (7). Lastly, combined male
186 and female *Chd4* βKO mice were significantly more glucose intolerant (Figure 2G) when
187 compared to control mice. Interestingly, the significant decrease in the insulin positive hormone
188 area at 3-weeks was not accompanied by a change in the total islet area between *Chd4* βKO and
189 control mice (Figure 2H).
190
191 *Chd4 βKO mice phenotype worsens through 6 weeks of age and are diabetic by 10 weeks of age*
192 By 6 weeks of age, fasting and *ad libitum* blood glucose levels in both the male and
193 female *Chd4* βKO mice were significantly elevated compared to controls (Figure 3A,
194 Supplementary Figure 4B). There was still a significant decrease in the insulin positive hormone
195 area between *Chd4* βKO mice and control mice, while both glucagon and somatostatin positive
196 hormone areas were unchanged (Figure 3B). At this age, islet architecture continued to be
197 disrupted with peripheral glucagon and somatostatin expressing cells present in the interior of the
198 islets, but there was still no evidence of polyhormonal cells (Figure 3C). Also at 6 weeks, the

*Chd4* βKO mice became progressively more glucose intolerant (Figure 3D), though the significant decrease in the insulin positive hormone area at 6 weeks was still not accompanied by a change in the total islet area between *Chd4* βKO and control mice (Figure 3E), suggesting β cells were maintained, but not expressing insulin.

By 10 weeks of age, the *Chd4* βKO male mice became severely diabetic compared to controls, displaying significantly lower body weight, significantly higher fasted and *ad libitum* blood glucose levels, severe glucose intolerance (Supplementary Figure 4C) and dehydration due to excessive urination. The hyperglycemic phenotype and health of the female mice also continued to worsen through 10 weeks of age (Supplementary Figure 4C), although the decline progressed more slowly, and female mice did not become as severely diabetic until approximately 15 weeks of age (data not shown). Overall, the *Chd4* βKO mice displayed a significant hyperglycemia phenotype with significantly reduced insulin expression and glucose intolerance starting as early as 3 weeks of age. *Chd4* βKO mice progressed to diabetes by 10-15 weeks of age. Further phenotypic and molecular analysis focused on the 3-week - 6-week timepoints to minimize secondary affects associated with the diabetic phenotype.

*Chd4 βKO mice have reduced insulin content and defective insulin secretion*

In our attempts to isolate islets to assess the functionality of *Chd4 β*KO β cells we identified a striking islet fragility phenotype; the isolated *Chd4 β*KO mutant islets rapidly dissociated upon manipulation. To initially circumvent this challenge, insulin content from intact whole pancreata isolated from 6-week-old mice was measured. *Chd4* βKO mice displayed significantly less insulin content compared to control mice (Figure 3F). To assess insulin secretion, live pancreas slices (28) were generated, and used to perform Glucose Stimulated Insulin Secretion (GSIS) assays. These experiments demonstrated that *Chd4* βKO islets had normal basal insulin secretion at 2mM glucose, trending lower insulin secretion at 11mM glucose, significantly lower insulin secretion at 20mM glucose and trending lower insulin secretion at 20mM glucose + KCl conditions compared to controls (Figure 3G). Taken together, these studies suggested that the *Chd4* βKO islets had both reduced insulin production and an impaired glucose response.

*Chd4 mutant β cells show immature transcriptional landscape*

Because CHD4 is a chromatin remodeling factor that interacts with NKX2.2, a transcription factor, it was important to identify the transcriptional defects that could explain the observed β cell dysfunction. To purify the β cell population we introduced an $Ins2^{(GFP/+)}$ allele (29) into the control and *Chd4* βKO mice for Fluorescence Activated Cell Sorting (FACS) (Supplementary Figure 5). Transcriptome analysis on β cells isolated from 4-week-old mice revealed a large number of genes significantly upregulated and downregulated in the *Chd4* βKO mice vs. controls (Figure 4A). Consistent with efficient conditional deletion of the *Chd4* locus, *Chd4* was one of the most significantly downregulated genes. In addition, there was a significant decrease in many essential β cell genes/factors including *Ucn3, MafA* and *Foxo1.* There was also a reduction in many of the genes involved in glucose sensing and insulin secretion including *Slc2a2* (GLUT2)*, Syt13, Ero1lβ, G6pc2*, *Slc30a8* (ZnT8), and *Glp1r* (Figure 4B). Interestingly, *Chd4* βKO mice also displayed a significant increase in genes normally expressed in immature β cells including *MafB* and *Npy* or pancreas disallowed genes such as *Hk1*. Consistent with the lack of polyhormonal cells in the IF analysis, there was not a corresponding increase in non-β endocrine cell genes. Lastly, we also observed significant downregulation of *Robo2* (Figure 4B). Previous studies demonstrated that deletion of *Robo1* and *Robo2* from β cells (*Robo* βKO) caused islets to easily dissociate (30, 31). Deletion of *Robo2* alone from the β cells was sufficient to disrupt the islet architecture (32, 33), similar to the phenotypes observed in the *Chd4* βKO mice. Overall, transcriptional analysis of the *Chd4* βKO β cells identified disruption of many β cell

maturity and functional markers suggesting this was the underlying cause of the severe CHD4 mutant phenotype.

*CHD4 affects NKX2.2 - associated β cell gene regulation through chromatin remodeling*

After identifying CHD4 as an NKX2.2 co-factor, we were specifically interested in β cell genes that were co-regulated by NKX2.2 and CHD4 and were associated with changes in the chromatin landscape when CHD4 was deleted. To detect changes in chromatin landscape, we reanalyzed a previously published CHD4 Control ATAC-seq vs. adult CHD4 βKO ATAC-seq dataset (22). As expected for a chromatin modifier protein, there were greater than 52,500 total peaks of significantly altered chromatin (padj < 0.05) when CHD4 was disrupted. The majority of peaks (39,956) displayed regions of more open chromatin, although there were a number of regions (12,843) that became more closed. To identify genes that are NKX2.2-dependent direct targets of CHD4, we identified genes that were bound by NKX2.2, dysregulated in both the *Nkx2.2* βKO and *Chd4* βKO islets and displayed changes in chromatin accessibility. 62 genes were present in all five datasets (Figure 4C), including *Ucn3, Slc2a2, G6pc2, Slc30a8, Kcnj5 and Npy,* suggesting that these genes represent potential direct targets of CHD4 and NKX2.2.

*β cell maturation genes are direct targets of NKX2.2 and CHD4*

To validate the subset of potential NKX2.2-dependent direct gene targets of CHD4 that correlated with the observed phenotypes, we performed chromatin precipitation followed by qPCR (ChIP-qPCR) in MIN6 cells on genes that either were deactivated or activated in the absence of CHD4 and NKX2.2. We included the previously characterized CHD4 bound *MafA* regulatory region 3 as a positive control for these experiments (21, 34). *Slc2a2,* the gene encoding the β cell glucose transporter GLUT2 is bound by NKX2.2, displayed reduced chromatin accessibility in the CHD4 βKO ATAC samples and was significantly down regulated when either *Nkx2.2* or *Chd4* were deleted from β cells (Figure 4D). Alternatively, *Kcnj5* (GIRK4), a channel that is normally not expressed in pancreatic β cells and responds to somatostatin and epinephrine signaling, is also bound by NKX2.2, had increased chromatin accessibility in the CHD4 βKO samples and was up regulated when either *Nkx2.2* or *Chd4* were deleted from β cells (Figure 4D). CHD4 ChIP-qPCR validated both genes were bound by CHD4 demonstrating they were direct targets that are co-regulated by NKX2.2 and CHD4 (Figure 4D, 4E). Closer analysis in a subset of genomic regions identified in these datasets, indicates that NKX2.2 binds to and facilitates the recruitment of CHD4 to alter the chromatin landscape to allow appropriate gene transcription.

*Chd4 mutant β cells show disrupted calcium signaling*

With the observed down regulation of *Robo2 in the Chd4* βKO islets, and previous research showing the deletion of *Robo1* and *Robo2* from β cells causes both fragile islets and disrupts calcium signaling (30), we next tested whether disrupted calcium signaling contributed to the insulin secretion defects. To circumvent the islet fragility phenotype, we tested calcium signaling in *Chd4* βKO islets using the live pancreas slice preparation (28). Using the $Ca^{2+}$ sensor, Fluo-4, we measured the $Ca^{2+}$ response in control and *Chd4* βKO pancreatic slices upon elevated glucose. Following addition of 11mM glucose, islets within control slices showed an initial elevation in $Ca^{2+}$, followed by synchronized pulsatile waves of $Ca^{2+}$ (Figure 5A, Supplementary Video 1), which is similar to the patterns seen in control isolated islets. However, the islets within *Chd4* βKO slices lacked any $Ca^{2+}$ response to elevated glucose, including lack of an initial elevation in $Ca^{2+}$, and lack of pulsatile waves of $Ca^{2+}$ (Figure 5B, Supplementary Video 2). The mean $Ca^{2+}$ elevation, expressed as the mean fluorescence increase from 0-5 minutes and 5-25 minutes each had significantly lower signal in the *Chd4* βKO slices than in the control slices (Figure 5C, 5D). Therefore, the *Chd4* βKO slices show a substantial decline in the $Ca^{2+}$ response

298 to glucose, which could cause the impaired glucose-stimulated insulin secretion and the overall
299 dysfunction of the *Chd4* βKO mutant β cells.
300
301 **Discussion**
302 β cell maturation is necessary to achieve proper glucose-responsive β cells and when
303 disrupted can cause dysfunction and loss of identity in β cells leading to hyperglycemia. Prior
304 studies in our lab have shown the essential role of NKX2.2 in the proper development, maturation
305 and function of pancreatic β cells. Given its diverse functions, NKX2.2 likely interacts with co-
306 factors to exert its activities. In this study, we identified about 200 proteins that potentially
307 interact with NKX2.2 to facilitate transcriptional regulation in the β cell. Many of the interactions
308 were mediated by either the TN domain, SD domain or both. The IP-MS successfully validated
309 previously characterized interactions between NKX2.2 and HDAC1, DNMT3A, and DNMT1 that
310 were facilitated through the NKX2.2 TN domain and function to repress non-β cell genes in β
311 cells (8). In addition, we identified novel interactions between NKX2.2 and several members of
312 the Nucleosome Remodeling and Deacetylase (NuRD) complex, including CHD4, an enzymatic
313 component of the complex. We initially theorized that the interaction between NKX2.2 and
314 CHD4 would facilitate transcriptional repressor activities that were mediated by the NKX2.2 TN
315 domain. However, the MS and Co-IP experiments suggested that the interaction with CHD4 is
316 predominantly mediated by the NKX2.2 SD domain. Deletion of *Chd4* from β cells affected both
317 the repression and activation of essential genes, leading to the disruption of the proper maturation
318 and function of β cells.
319 Although *Chd4* was deleted from β cells at the onset of insulin expression at
320 approximately gestational embryonic stage e12.0, the *Chd4* βKO mice did not display an overt
321 phenotype at P2, suggesting the lack of an overt developmental phenotype. This result was
322 somewhat surprising given its interaction with NKX2.2, which is essential for proper β cell
323 development (4, 5). It is possible that *Chd4* is dispensable for embryonic β cell development.
324 Alternatively, although we confirmed that CHD4 was efficiently removed from the majority of
325 the adult β cells (Supplementary Figure 2B), a small proportion of β cells retained CHD4
326 expression and these remaining β cells could be sufficient to sustain glucose regulation through
327 the early postnatal stages. Alternatively, CHD4 function may also be compensated by other
328 family members including CHD3 and CHD5, which were both upregulated in the *Chd4* βKO
329 (Figure 4B). However, if CHD3 and CHD5 do compensate for CHD4 during the developmental
330 window, they appear to be unable to fully do so in β cell maturation and function postnatally.
331 Deletion of *Chd4* from the developing β cell lineage had a substantial impact on the
332 maturation and function of β cells. *Chd4* βKO mice were glucose intolerant and hyperglycemic by
333 3 weeks of age with their symptoms worsening with age. Interestingly, a recent study that used a
334 *MIP:Cre*$^{ERT}$ to remove *Chd4* from fully mature adult β cells (22) caused impaired insulin
335 secretion; however, the phenotype was less severe than when *Chd4* was deleted from developing
336 β cells, suggesting that in β cells CHD4 may play a stronger role in initiating chromatin
337 modifications to establish a transcriptional program than maintaining chromatin structure. In
338 addition, several important β cell transcription factors, including *Foxo1*, and β cell maturation
339 factors such as *Ucn3* were not affected when *Chd4* was deleted from adult β cells, suggesting that
340 maintenance of β cell identity and maturation is not dependent on CHD4. However, *Robo2* and
341 *Slc2a2* gene transcription was disrupted in the *Chd4*$^{fl/fl}$*; MIP:Cre*$^{ERT}$ mice, suggesting CHD4 is
342 required to maintain β cell integrity and functional status.
343 This study begins to parse out novel roles of CHD4 in establishing the correct chromatin
344 landscape and transcriptional status during the formation and maturation of β cells vs. its role in
345 maintaining β cell functions. Davidson et al., (21) identified an interaction between CHD4 and
346 PDX1 and showed the interaction of CHD4 facilitated by PDX1 may also be tuned through
347 glucose sensing in the β cell. Though we have not determined if NKX2.2 and CHD4's interaction

348 is facilitated through glucose sensing, the NKX2.2 MS did identify PDX1 as a potential NKX2.2
349 interacting factor. Consistently, NKX2.2 and PDX1 co-regulate many essential regulatory sites in
350 the β cell genome including at *Mafa, Slc2a2 and Robo2,* although not all sites are shared, such as
351 at *Kcnj5* (7, 35). This leads us to believe that some actions of CHD4 in the β cells are facilitated
352 through its recruitment from both NKX2.2 and PDX1. Further work is needed to determine when
353 CHD4 is recruited solely by NKX2.2, PDX1 or both and how this differential recruitment affects
354 its molecular functions.
355 At the end of the pancreatic β cell maturation window, at approximately 3 weeks of age,
356 the *Chd4* βKO mice were glucose intolerant with elevated blood glucose levels and a reduction in
357 the insulin area. Since there was not a substantial change in total islet area in these mutant mice
358 (Figure 2H, 3E), the observed reduction in insulin positive area was most likely caused by a
359 reduction in insulin production rather than a decrease in β cell numbers. Consistently, we did not
360 observe changes in Ki-67 staining for proliferation or TUNEL staining for cell death between
361 *Chd4* βKO and control mice (Supplementary Figure 6A, 6B). We were unable to perform lineage
362 tracing experiments to fully characterize whether β cells were still present but not producing
363 insulin because the *R26R:tdTomato* locus is closely linked to the *Chd4* locus on mouse
364 chromosome 6 precluding our ability to generate a $Chd4^{(fl/fl)}$; $Ins1^{(Cre/+)}$; $Rosa^{(Tomato/Tomato)}$ lineage
365 tracing mouse.
366 The identification of *Robo2* as significantly down regulated in the absence of Chd4,
367 suggests that loss of *Robo2* may contribute to the fragile islet phenotype as well as the disrupted
368 islet architecture and impaired calcium signaling (30, 32, 33). However, deletion of *Robo2* alone
369 from β cells did not cause disruption of maturation and β cell identity markers, which is seen in
370 our study. This suggests the loss of β cell maturation and identity may be driven by direct targets
371 of CHD4 such as *MafA* and *Slc2a2.* Furthermore, in addition to *Robo2*, multiple genes involved in
372 cell-to-cell and cell-to-matrix junctions were also significantly down-regulated including many
373 genes involved in desmosomes (*Jup, Pkp2, Dsc2*) which have been shown to affect tissue
374 architecture and structure (36-38), suggesting additional CHD4 targets may contribute to the
375 fragile islet phenotype. Lastly, the upregulation of *Kcnj5* could contribute to the disrupted calcium
376 signaling as well. *Kcnj5* encodes the GIRK4 channel, which is not normally expressed in β cells
377 but can respond to somatostatin and epinephrine signaling. These signals can potentially hyper-
378 polarize the β cell, affecting calcium signaling and insulin secretion (39).
379 In other tissue and cell types, CHD4 has been shown to either activate genes, including
380 those associated with lineage programs (16, 17), or repress genes associated with alternative
381 lineage programs (14, 40). We have shown that in pancreatic β cells, CHD4 has the ability to bind
382 at and either activate or repress transcription of β cell genes. NKX2.2 facilitates the ability of
383 CHD4 to bind at and manipulate the chromatin state at certain genes, allowing CHD4 to activate
384 essential maturation and functional β cell genes, such as *Slc2a2* while at the same time repressing
385 genes that will be detrimental to β cell function, such as *Kcnj5*. However, we did observe nearly
386 1000 more genes up regulated overall with the deletion of *Chd4* as well as almost three times the
387 number of regions that gained open chromatin in the CHD4 βKO ATAC-seq. This suggests that
388 although CHD4 can both activate and repress genes in β cells, CHD4 is still primarily acting as a
389 repressor. Additional studies would be necessary to identify whether the distinct NKX2.2
390 domains confer either NKX2.2 and/or CHD4 combined roles as repressors or activators in β cells.
391 It is possible that HDAC1 and the NuRD complex are recruited by the NKX2.2 TN domain to
392 repress certain β cell genes, whereas activation of a different subset of β cell genes via CHD4 is
393 facilitated by the NKX2.2 SD domain.
394 Overall, understanding the transcriptional network that facilitates the proper development,
395 maturation and function of pancreatic β cells can help lead to better treatment options for diseases
396 like diabetes. This study increases our understanding of how essential transcription factors in the

397 β cell, like NKX2.2, maintain a proper transcriptional state through the interaction with cofactor
398 proteins such as CHD4 to allow the proper maturation and function of β cells.
399
400 **Materials and Methods**
401
402 *Cell Line and Cell Culture*
403 Mouse Insulinoma (MIN6) β cell culture line was originally created by the Yamamura lab
404 (41) and cultured at 37°C and 5% $CO_2$. MIN6 cells were passaged every 7 days and fed media
405 containing Dulbecco's Modified Eagle Medium (DMEM) high glucose, with L-glutamine,
406 without Sodium pyruvate and HEPES (Gibco, Cat. # 11965-092) and supplemented with 10%
407 FBS (Gibco, Cat. #A5669701), 5% PenStrep (10,000U/mL Penicillin-Streptomycin, Gibco, Cat.
408 #15140-122) and .00040% βME.
409
410 *Nkx2.2 Domain Variant Plasmid Transfections*
411 MIN6 cells were forward transfected with 31.5 µg of one of the following *Nkx2.2*
412 plasmids: pcDNA3-3x Myc-EV, pcDNA3-3x Myc-Nkx2.2 WT, pcDNA3-3x Myc-Nkx2.2 $TN^{mut}$,
413 pcDNA3-3x Myc-Nkx2.2 $SD^{mut}$, or pcDNA3-3x Myc-Nkx2.2 $SD^{mut}$ / $TN^{mut}$. Lipofectamine-3000
414 was used as the transfection reagent (Invitrogen, Cat. #L3000015) and MIN6 cells were
415 transfected for 72 hours prior to protein extraction using the Nuclear Extract Kit (Active Motif,
416 Cat. #40010). Protein concentration was assessed using the DC assay kit (Bio-Rad, Cat.
417 #5000112).
418
419 *Co-Immunoprecipitation for Mass Spectrometry*
420 For mass spectrometry (mass spec) of transfected Myc tagged NKX2.2 proteins, pull
421 downs were performed by incubating Anti-c-MYC magnetic beads (Pierce, Cat. #88843) with
422 samples for 1 hour with mixing at 4°C. Samples were then washed with a Co-IP Buffer (50mM
423 HEPES, 1mM EDTA, 5% glycerol, 0.5% Triton-X, 500nM NaCl). For mass spec of endogenous
424 CHD4 protein, pulldowns were performed in WT MIN6 cells using the Nuclear Complex Co-IP
425 Kit (Active Motif, Cat. #54001) per the manufacturer's instructions. Briefly, 500 µg of WT MIN6
426 nuclear extract was incubated in IP High Buffer (no detergent and no NaCl) using 5 µg of CHD4
427 rabbit antibody (D8B12, CST, Cat. #11912) or 5 µg of a control IgG rabbit antibody (CST, Cat.
428 #2729), overnight with mixing. The second day, samples were incubated with Anti-Protein-A
429 magnetic beads (Pierce, Cat. #88846) for 1 hour with mixing at 4°C. Samples were then washed
430 using the IP High Buffer (no detergent and no NaCl) with and without BSA.
431 For both the NKX2.2 and CHD4 samples, 4x Laemmli buffer (Bio-rad, Cat. #1610747)
432 plus βME was used as a sample buffer and samples were boiled for 5 minutes at 95°C and loaded
433 in a Bio-Rad Mini-PROTEAN TGX Gel (4-20%, 10-well, 50 µL, Bio-rad, Cat. # 456-1094).
434 Once all samples had collected into compact bands in the stacking gel portion, the gel was
435 stopped and extracted and washed 3x for 5 minutes in Milli-Q water. The gel was stained in
436 SimplyBlue SafeStain (Invitrogen, Cat. # LC6060) for 1 hour at RT. The gel was destained 2x for
437 1 hour in Milli-Q water . The gel bands were cut out and submitted to the mass spec core in
438 microcentrifuge tubes filled with water for processing. pcDNA3-3x Myc-EV was used as the
439 control sample in the NKX2.2 experiment and IgG was used as the control sample in the CHD4
440 experiment.
441
442 *NKX2.2 & CHD4 Mass Spectrometry*
443 Samples were tryptically digested prior to LC/MS/MS analysis according to an established
444 protocol (42, 43). Briefly, under keratin-free conditions, stacking gel bands were excised from the
445 gel and dehydrated before being incubated with 25 ng/µL of trypsin at 37°C for 18 hrs, after
446 which the enzyme was deactivated with 10% formic acid (FA). Peptides were extracted from the

447 gel fragments, dried via speedvac, and resuspended for mass spectrometric analysis. NKX2.2
448 samples were re-suspended in 20 µL of buffer and CHD4 samples were re-suspended in 14 µL of
449 buffer. NKX2.2 samples were analyzed similar to a previous publication (44), with the following
450 exceptions: MS/MS data was collected in positive ion polarity over mass ranges 260–1700 m/z at
451 a scan rate of 8 spectra/second for MS scans and mass ranges 50–1700 m/z at a scan rate of 3
452 spectra/second for MS/MS scans.
453 2 µL of CHD4 samples were acquired on an Orbitrap Eclipse (Thermo Scientific)
454 operated using intensity-dependent CID MS/MS to generate peptide ID's and equipped with a
455 Ultimate 3000 RSCLnano LC system (Thermo Scientific) using a previously published method
456 with the following exceptions: The orbitrap MS1 scan mass range was set to 375-1500 m/z range
457 and dynamic exclusion was set to 20 seconds instead of 14 seconds (45). PEAKS studio
458 proteomics version 10.5 was used to extract, search, and summarize peptide identity results from
459 IgG and CHD4 samples (PEAKS, Waterloo, ON, Canada). Peptide identifications were
460 performed using the PEAKS DB search engine combined with PEAKS de novo sequencing.
461 Extracted spectra were searched against the SwissProt Mus musculus database. The crude PEAKS
462 studio proteomics extractor protein abundance levels were used to compare relative abundances
463 of proteins in each sample to determine protein interactors for CHD4.
464
465 *Co-Immunoprecipitation and Western Blotting*
466 For Co-IP and western of endogenous CHD4, pulldowns were performed in WT MIN6
467 cells using the Nuclear Complex Co-IP Kit (Active Motif, Cat. #54001) per the manufacturer's
468 instructions. Briefly, 500 µg of WT MIN6 nuclear extract was incubated in IP High Buffer (no
469 detergent and no NaCl) using 5 µg of CHD4 rabbit antibody (D4B7, CST, Cat. #12011) or 5 µg
470 of a control IgG rabbit antibody (CST, Cat. #2729), overnight with mixing. The second day,
471 samples were incubated with Anti-Protein-A magnetic beads (Pierce, Cat. #88846) for 1 hour
472 with mixing at 4°C. Samples were then washed using the IP High Buffer (no detergent and no
473 NaCl) with and without BSA. For all samples, including 5% input samples, 2x Laemmli buffer
474 (Bio-rad, Cat. #1610737) plus βME was used as a sample buffer and samples were boiled for 5
475 minutes at 95°C and loaded in a Bio-Rad Mini-PROTEAN TGX Gel (4-20%, 10-well, 50 µL,
476 Bio-rad, Cat. # 456-1094) with a Precision Plus Protein Ladder (Bio-rad, Cat. #1610375). Protein
477 gels were transferred onto PVDF membranes and washed 3x for 5 minutes in TBS-T at RT.
478 Membranes were blocked in TBS-T + 5% milk for 1 hour at room temp and membranes were
479 washed 3x for 5 minutes in TBS-T at RT. Primary antibodies (Supplemental Table #2) were
480 added at concentrations noted in TBS-T + 5% BSA overnight on a rocker at 4°C. The next day,
481 membranes were washed 3x for 5 minutes in TBS-T at RT and an IP Veriblot HRP secondary
482 antibody was added at 1:500 in TBS-T + 5% Milk (abcam, Cat. #ab131366). Membranes were
483 washed 3x for 5 minutes in TBS-T at RT and imaged using SuperSignal West Pico PLUS
484 Chemiluminescent Substrate (Thermo Scientific, Cat. #34580).
485
486 *Mouse Islet Western Blotting*
487 For western blot of endogenous CHD4 in mouse islets, islets from 3 mice of control or
488 mutant genotype were isolated as described above and were pooled to form 1 control or mutant
489 sample. Islets were lysed using 1x RIPA Buffer (Abcam, Cat. # 156034) + PIC tablets
490 (Invitrogen, Cat. # A32961) for 30 minutes on ice. Samples were spun down at 12,000 rpm for 20
491 minutes at 4°C and protein concentration was assessed using the DC assay kit (Bio-Rad, Cat.
492 #5000112). 50 µg of Control or Mutant Mouse Islet Lysate was used and western was run as
493 described above. Vinculin was used as the loading control (Supplemental Table #2).
494
495 *Generation of Chd4 KO Mice and Animal Maintenance*

496 *Chd4* pancreas KO mutant mice were created by breeding *Pdx1*$^{(Cre/+)}$ mice (B6.FVB-
497 Tg(Pdx1-cre)6Tuv/J) (23) and *Chd4*$^{(flox/flox)}$ (Chd4$^{tm1.1Kge}$) created in the Georgopoulos lab (16).
498 *Chd4* βKO mutant mice were created by breeding *Ins1*$^{(Cre/+)}$ mice (B6(Cg)-*Ins1*$^{tm1.1(cre)Thor}$/J) (24)
499 and *Chd4*$^{(flox/flox)}$ mice. For experiments requiring cell sorting, *Ins2*$^{(GFP/+)}$ reporter mice (29) were
500 bred into the *Chd4* control and βKO line. Physiological studies were conducted on male and
501 female mice with ages of mice being noted for each experiment. Mice were kept in accordance
502 with University of Colorado Institutional Animal Care and Use Committee (IACUC) protocol
503 #00045. Genotyping primers are listed in Supplemental Table #1.
504
505 *Blood Glucose Readings*
506 Fasted blood glucose was measured after a 6 hour fast from mouse tail vein. *Ad libitum*
507 blood glucose readings were taken from the mouse tail vein of fed mice. All glucose readings
508 were taken using a Contour 7151H glucose meter and Contour 7097C test strips.
509
510 *Glucose Tolerance Test*
511 Mice were fasted for 6 hours and initial blood glucose readings were taken at timepoint 0
512 from mouse tail vein. Mice were then injected with 2mg per gram of body weight D-glucose
513 (Sigma, Cat. #G8270-1Kg). Additional tail vein blood glucose readings were taken at time 15, 30,
514 60, 90 and 120 minutes. All glucose readings were taken using a Contour 7151H glucose meter
515 and Contour 7097C test strips. The area under the curve was analyzed using PrismGraphPad
516 10.4.1.
517
518 *Mouse Pancreas Tissue Preparation and Immunofluorescence Staining*
519 Mouse pancreata were dissected at specified ages and fixed in 4% PFA for 4 hours.
520 Following fixation, pancreata were placed in 30% sucrose overnight then embedded in Optimal
521 Cutting Temperature (OCT) Compound (Sakura, Cat. #4583) and frozen at -80°C. Tissue blocks
522 were sectioned using a cryostat (Thermo Microm525) at a slice thickness of 10µm. Three
523 consecutive slices were added to each slide until the entire pancreas was sectioned completely
524 through, around 100-120 slides total.
525 For immunofluorescent staining, every 10$^{th}$ slide, covering the entire pancreas was stained.
526 Prior to staining, slides were thawed for 10 minutes. If antigen retrieval was necessary slides were
527 preheated with Na Citrate (10mM Na Citrate, 0.05% Tween, pH 6.00) and heated for 20 minutes
528 followed by washes using PBS-T (0.1% Tween-20). Slides were then blocked using PBS-T + 2%
529 Normal Donkey Serum (NDS) at room temperature (RT) for 30 minutes. Slides were washed 1x
530 in PBS-T for 5 minutes at RT followed by addition of primary antibodies (Supplemental Table
531 #2). Slides were incubated overnight at 4 degrees in humid chamber. The following day slides
532 were washed 4x in PBS-T for 5 minutes at RT followed by addition of secondary antibodies
533 (1:500 in PBS-T + 2% NDS). Secondary antibodies were incubated on slides for 1-3 hours in
534 humid chamber at RT. Slides were washed 4x in PBS-T for 5 minutes at RT followed by addition
535 of DAPI (1:1000 in PBS-T) and incubated for 15 minutes at RT. Slides were washed 2x in PBS-T
536 for 5 minutes at RT followed by addition of Prolong Gold mounting reagent (Invitrogen P36930),
537 22x60 cover slips and sealed using clear nail polish (Electron Microscopy Sciences, Cat. #72810).
538
539 *Image Analysis and Quantification*
540 For the P2, 3 week and 6-week timepoints, images were taken on a Leica DM5500B with
541 a Leica DFC 345 FX and Leica DFC425 camera. Filters cubes were A4, L5 and N3. For the P2
542 timepoint, pictures of entire pancreas sections were taken using the tilescan function using the 10x
543 objective. For the 3-week and 6-week timepoints, pictures of all individual islets were taken using
544 a 20x objective from one of the three pancreas slices of each slide stained. Each islet
545 immunofluorescent image was quantified using ImageJ2 Version 2.14.0/1.54f. Full islet area was

546 quantified as well as positive hormone area by quantifying all area above a set threshold (50 for
547 all channels). Hormone area for P2 was normalized by total pancreas area and hormone area for
548 3- and 6-week timepoints was normalized by total islet area. For all other immunofluorescent
549 staining images, images were taken on a Zeiss LSM 800 with the objective specified and using a
550 405, 488, 561 and 640 nm laser line.
551
552 *Whole Mouse Pancreas Acid Ethanol Insulin Collection*
553 10-20 mg sections of whole mouse pancreatic tissue were removed from both controls and
554 *Chd4* βKO mutant mice and placed in 1 mL of 0.18M HCl in 70% EtOH (acid ethanol) and
555 sonicated 2 x 30 seconds (Fisher Scientific Cat. #FS30H) and vortexed for 1 minute. Whole
556 pancreas tissue was incubated at 4°C for 12 hours and stored at -80°C until ELISAs were
557 performed using Mercodia Insulin ELISA (Cat. #10-1247-01) or Mercodia ProInsulin ELISA
558 (Cat. #10-1232-01) per the manufacturer's instructions.
559
560 *Generation of Full Mouse Pancreas Slices*
561 Pancreas tissue slices were prepared as previously described (28). Briefly, animals were
562 injected with 100 mg/kg ketamine and 8 mg/kg xylazine and euthanized via exsanguination prior
563 to inflating the pancreas with low-melting-point 1.25% agarose solution dissolved in extracellular
564 solution (ECS, consisting in 140 mM NaCl, 5 mM KCl, 2 mM $NaHCO_3$, 1 mM $NaH_2PO_4$, 1.2
565 mM $MgCl_2$, 1.5 mM $CaCl_2$, 3 mM glucose and 10 mM HEPES [pH is adjusted to 7.4 with
566 NaOH]) at 37°C into the common bile duct. Immediately after injection, the agarose infused
567 pancreas was cooled with ice-cold ECS, excised, trimmed into smaller blocks and embedded in
568 1.25% agarose. Tissues were sliced with a thickness of 200 µm with a vibratome (VF-310-0Z,
569 Precisionary) and collected in ice-cold ECS. Slices were then placed in a 24-well plate containing
570 1 ml/well of ECS with Soybean Trypsin (Final concentration 0.1 mg/ml) inhibitor to prevent any
571 inadvertent degradation by digestive enzymes. Slices were washed on an orbital shaker at 4°C for
572 1-hour prior to selection of islet containing slices. Slices were then placed in cell culture inserts
573 coated with a collagen mixture (28) in a 6-well plate with 2 ml of RPMI medium supplemented
574 with 10% FBS, 1% Pen-Strep, and trypsin inhibitor (Final Concentration 0.1 mg/ml), and kept
575 overnight in the Incubator at 37°C and 5% $CO_2$. Slices were then used to perform Glucose
576 Stimulated Insulin Secretion (GSIS) and intracellular calcium imaging experiments.
577
578 *Mouse Pancreas Slices Glucose Stimulated Hormone Secretion Assays and Analysis*
579 Insulin was assayed using static hormone secretion assays. All solutions were prepared in
580 Krebs-Ringer buffer (108.8 mM NaCl, 5 mM $NaHCO_3$, 5.8 mM KCl, 1.2 mM $KH_2PO_4$, 2.5 mM
581 $CaCl_2$, 1.2 mM $MgSO_4$, 10 mM HEPES, 0.1% BSA, pH 7.4) and supplemented with either 2mM,
582 11mM, or 20 mM Glucose and 20mM, 11 mM, or 2 mM NaCl for osmotic balance. Duplicate sets
583 of 3 or 5 pancreatic slices per condition were incubated in 2 mL of Krebs-Ringer buffer
584 containing 2 mM glucose for 1 hour to establish baseline secretion. Then, each slice set was
585 placed under a sequential 30-minute stimulation condition under one of three conditions: (1) 2
586 mM glucose, (2) 11 mM glucose, or (3) 20 mM glucose. A final 30-minute stimulation was
587 performed with 20 mM + KCl in addition to each respective glucose/NaCl condition. After each
588 30-minute stimulation, 500 µL of supernatant was collected for analysis. Samples were stored at
589 -20°C until analysis. Insulin concentrations were measured using a mouse ultrasensitive insulin
590 ELISA kit (Crystal Chem, Cat. #90096) per the manufacturer's instructions.
591
592 *Mouse Islet Isolation and Dissociation*
593 Islets were isolated by the Islet Isolation Core facility. Briefly, mice were anesthetized
594 using a ketamine/xylazine/acepromazine (KXA) mixture and euthanized by exsanguination. The
595 pancreatic duct was clamped off and a 26-gauge needle with a collagenase mixture was injected

596 into the pancreas. The pancreas was dissected out of the mouse and islets were isolated by a
597 density gradient purification step followed by hand picking.
598 After isolation, islets were collected and placed in a 15mL tube and allowed to settle for
599 20 minutes. Islets were washed with pre-warmed PBS and spun at 300 x g for 3 minutes at RT.
600 PBS was aspirated off and islets were resuspended in 2 mL of Accutase (Stemcell Tech, Cat.
601 #07920) and placed in a 37°C water bath. Islets were incubated for 30 minutes total, resuspending
602 islets by pipetting every 5 minutes. Accutase dissociation was stopped by adding RPMI1640
603 (Gibco, Cat. #11875-093) + 10% FBS. Dissociated islet cells were filtered through a 40µm cell
604 strainer (Greiner, Cat. #542040) into a 50mL conical tube. Cells were spun at 300 x g for 3
605 minutes at RT. Supernatant was carefully aspirated off without disturbing cell pellet and cells
606 were washed in 10mL FACS buffer (PBS + 1mM EDTA + 0.2% BSA). Cells were spun at 300 x
607 g for 3 minutes at RT, supernatant was aspirated off and cells were resuspended in 1mL of FACS
608 buffer for sorting. Propidium Iodide (PI, Thermo Cat. #P3566) was added as a live/dead marker at
609 1:1000.
610
611 *Mouse Islet β Cell Fluorescent Activated Cell Sorting (FACS)*
612 β cells were sorted from dissociated 4 week mouse islets using an *Ins2*$^{(GFP/+)}$ reporter (29)
613 on a Bio-rad S3e cell sorter. Gates were set to initially read FSC and SSC area to sort out debris
614 and cell doublets. Cells were then gated using a PI negative to separate out living vs dead cells
615 and lastly cells were gated using a GFP positive gate to sort and collect all β cells (Supplementary
616 Figure 5). Cells were collected in 350 µL of RLT Lysis buffer + βME (Qiagen RNeasy Micro Kit,
617 Cat. #74004), prior to RNA extraction.
618
619 *RNA Extraction and RNA Sequencing*
620 RNA extraction was performed using the RNeasy Micro Kit (Qiagen, Cat. 74004)
621 protocol. 2-Mercaptoethanol (βME) was added to RLT lysis buffer to help inhibit RNases. RNA
622 quality was assessed using an Agilent 4200 TapeStation System and RNA samples with RNA
623 Integrity Numbers (RIN) scores of 8 or higher were used for sequencing. RNA samples were
624 sequenced at the Genomics Core facility on the University of Colorado Anschutz Medical
625 Campus. Paired end libraries were made by the core from low input ribo-depleted RNA using
626 SMARTer Stranded Total RNA-Seq Kit v2 – Pico Input Mammalian (Takara Cat.# 634411). All
627 libraries were run on a NovaSEQ X machine at a sequencing depth of 50 million read pairs / 100
628 million total reads per sample. Fastq files were quality checked using FastQC (v0.12.1) (46) and
629 adapters were trimmed using Cutadapt (v4.8) (47). The reads were mapped to the mm10 genome
630 using STAR (v2.7.11a) (48). Counts tables were made using featureCounts (v2.0.6) (49) and used
631 for differential gene expression analysis. Differential genes were assessed using DESeq2
632 (v1.46.0) (50) and significant genes were established using a padj value of $\leq 0.05$ and a $Log_2$ Fold
633 Change value of $> 0.5$ or $< 0.5$.
634
635 *Reanalysis of ATAC-seq Dataset*
636 The reanalysis of the published ATAC-seq data (22) was conducted by downloading Fastq
637 files from the GEO database under reference number GSE217444. Files were processed using our
638 bulk ATAC-seq snakemake pipeline. Briefly, Fastq files were quality checked using FastQC
639 (v0.12.1) (46) and adapters were trimmed using Cutadapt (v4.8) (47). The reads were aligned to
640 the mm10 genome using Bowtie2 (v2.5.3) (51) and mitochondrial reads were removed using
641 Samtools (v1.20) (52). The ATACseqQC package (v1.28) (53) was used to generate final quality
642 metric plots, and FRiP values were tabulated using featureCounts (v2.0.6) (49). We used MACS3
643 (v3.0.2) (54) with a q-value cutoff of 0.01 to call peaks within the dataset, then utilized DiffBind
644 (v3.14) (55) with DESeq2 (v1.46.0) (50) and a padj value $< 0.05$ to identify differentially
645 accessible peaks between the CHD4 Control and CHD4 βKO ATAC-seqs.

*CHD4 ChIP-qPCR*

20 million MIN6 cells were collected for use in the SimpleChIP Enzymatic Chromatin IP Kit (Magnetic Beads, CST, Cat. #9003) per the manufacturer's instructions. Briefly, cells were crosslinked with 1% formaldehyde for 10 minutes and crosslinking was quenched with glycine. Cells were lysed and chromatin was fragmented using a Diagenode Bioruptor Pico sonicator and Micrococcal Nuclease (CST, Cat. # 10011) to fragment chromatin to approximately 150-900bp. 2% of samples was removed to be used as input before pulling down CHD4. 30 µg of fragmented chromatin DNA was used for IP with 10 µL CHD4 antibody (Rabbit, CST D4B7, 12011S) or 2µL IgG (Rabbit, CST, Cat. #2729). Samples were next incubated overnight with rotation at 4°C and 30 µL of ChIP-Grade Protein G Magnetic Beads (CST, Cat. #9006) was added, followed by incubating samples again for 2 hours with rotation at 4°C. Chromatin was eluted from beads and cross-links were reversed using NaCl, RNase A and Proteinase K and DNA was purified from samples using DNA spin columns.

For qPCR, 3 replicates of 5 ng of CHD4 IP or IgG IP samples were used with iTaq Universal SYBR Green Supermix (Bio-Rad, Cat. #1725120) and primers (Supplementary Table #1). A Bio-Rad CFX96 system was used to run qPCR plate. Fold enrichment over IgG was used to quantify CHD4 binding over IgG control.

*Mouse Pancreas Slices Calcium Signaling and Analysis*

Slices were incubated with 4 µM Fluo-4 AM (Thermo Fisher Scientific Cat. #F14201) in BMHH buffer containing 125 mM NaCl, 5.7 mM KCl, 2.5 mM $CaCl_2$, 1.2 mM $MgCl_2$, 10 mM HEPES, 0.1% bovine serum albumin (BSA), 2 mM glucose, and 1mg/ml Trypsin inhibitor at room temperature for 30 min in the dark. Slices were transferred to MatTek glass-bottom imaging dishes (MatTek, Cat. #P35G-1.5-14-C) with fresh BMHH with 2 mM glucose prior to imaging. An anchor was placed to hold the slice in place. Slices were imaged on a Zeiss laser scanning microscope (LSM) 800 with a 40x objective using a 488 nm laser. Slices were imaged at 37°C, where images were acquired every second for 2.5–5 min at 2mM glucose. Following imaging, medium was changed to 11 mM glucose and images were acquired for another 15-30 min. Fiji was used to extrapolate the calcium time courses. The time courses were normalized for intensity and normalized for movement if needed. The area under the curve was analyzed using PrismGraphPad 10.4.1.

*Statistical Analysis*

Unless otherwise stated, error bars are shown as mean +/- standard deviation (SD) and Shapiro-Wilk test was used to test normality. If passed, unpaired two-tailed student's t-test was used to determine significant differences, otherwise, Mann-Whitney U test was used. P-value or padj of $\leq$ 0.05 was used to determine statistical significance. If no statistics are shown on graphs, results were not significant.

**References**

1. M. C. Jorgensen, J. Ahnfelt-Ronne, J. Hald, O. D. Madsen, P. Serup, J. Hecksher-Sorensen, An illustrated review of early pancreas development in the mouse. *Endocr Rev* **28**, 685-705 (2007).
2. L. C. Murtaugh, Pancreas and beta-cell development: from the actual to the possible. *Development* **134**, 427-438 (2007).
3. F. C. Pan, C. Wright, Pancreas organogenesis: from bud to plexus to gland. *Dev Dyn* **240**, 530-565 (2011).

4. K. J. Sussel L, Hartigan-O'Connor DJ, Meneses JJ, Pedersen RA, Rubenstein JL, German MS, Mice lacking the homeodomain transcription factor Nkx2.2 have diabetes due to arrested differentiation of pancreatic beta cells. *Development* (1998).
5. M. J. Doyle, Z. L. Loomis, L. Sussel, Nkx2.2-repressor activity is sufficient to specify alpha-cells and a small number of beta-cells in the pancreatic islet. *Development* **134**, 515-523 (2007).
6. Sarah, Elisa, Hana, M. Zerah, Majedah, Julie, H. Stewart, E. Alamiri, K. Hussain, S. Wallis, Liat, O. Rubio-Cabezas, Jayne, Emma, A.-M. Patch, S. Ellard, Andrew, Analysis of Transcription Factors Key for Mouse Pancreatic Development Establishes NKX2-2 and MNX1 Mutations as Causes of Neonatal Diabetes in Man. *Cell Metabolism* **19**, 146-154 (2014).
7. G. D. Gutierrez, A. S. Bender, V. Cirulli, T. L. Mastracci, S. M. Kelly, A. Tsirigos, K. H. Kaestner, L. Sussel, Pancreatic beta cell identity requires continual repression of non-beta cell programs. *J Clin Invest* **127**, 244-259 (2017).
8. J. B. Papizan, R. A. Singer, S. I. Tschen, S. Dhawan, J. M. Friel, S. B. Hipkens, M. A. Magnuson, A. Bhushan, L. Sussel, Nkx2.2 repressor complex regulates islet beta-cell specification and prevents beta-to-alpha-cell reprogramming. *Genes Dev* **25**, 2291-2305 (2011).
9. V. Abarinov, J. A. Levine, A. J. Churchill, B. Hopwood, C. S. Deiter, M. A. Guney, K. L. Wells, J. M. Schrunk, Y. Guo, J. Hammelman, D. K. Gifford, M. A. Magnuson, H. Wichterle, L. Sussel, Major beta cell-specific functions of NKX2.2 are mediated via the NK2-specific domain. *Genes Dev* **37**, 490-504 (2023).
10. S. Dhawan, S. Georgia, S. I. Tschen, G. Fan, A. Bhushan, Pancreatic beta cell identity is maintained by DNA methylation-mediated repression of Arx. *Dev Cell* **20**, 419-429 (2011).
11. A. O'Shaughnessy-Kirwan, J. Signolet, I. Costello, S. Gharbi, B. Hendrich, Constraint of gene expression by the chromatin remodelling protein CHD4 facilitates lineage specification. *Development* **142**, 2586-2597 (2015).
12. H. Zhao, Z. Han, X. Liu, J. Gu, F. Tang, G. Wei, Y. Jin, The chromatin remodeler Chd4 maintains embryonic stem cell identity by controlling pluripotency- and differentiation-associated genes. *J Biol Chem* **292**, 8507-8519 (2017).
13. C. M. Wilczewski, A. J. Hepperla, T. Shimbo, L. Wasson, Z. L. Robbe, I. J. Davis, P. A. Wade, F. L. Conlon, CHD4 and the NuRD complex directly control cardiac sarcomere formation. *Proc Natl Acad Sci U S A* **115**, 6727-6732 (2018).
14. T. Arends, C. Dege, A. Bortnick, T. Danhorn, J. R. Knapp, H. Jia, L. Harmacek, C. J. Fleenor, D. Straign, K. Walton, S. M. Leach, A. J. Feeney, C. Murre, B. P. O'Connor, J. R. Hagman, CHD4 is essential for transcriptional repression and lineage progression in B lymphopoiesis. *Proc Natl Acad Sci U S A* **116**, 10927-10936 (2019).
15. J. V. Goodman, T. Yamada, Y. Yang, L. Kong, D. Y. Wu, G. Zhao, H. W. Gabel, A. Bonni, The chromatin remodeling enzyme Chd4 regulates genome architecture in the mouse brain. *Nat Commun* **11**, 3419 (2020).
16. C. J. Williams, T. Naito, P. G. Arco, J. R. Seavitt, S. M. Cashman, B. De Souza, X. Qi, P. Keables, U. H. Von Andrian, K. Georgopoulos, The chromatin remodeler Mi-2beta is required for CD4 expression and T cell development. *Immunity* **20**, 719-733 (2004).
17. S. Bornelov, N. Reynolds, M. Xenophontos, S. Gharbi, E. Johnstone, R. Floyd, M. Ralser, J. Signolet, R. Loos, S. Dietmann, P. Bertone, B. Hendrich, The Nucleosome Remodeling and Deacetylation Complex Modulates Chromatin Structure at Sites of Active Transcription to Fine-Tune Gene Expression. *Mol Cell* **71**, 56-72 e54 (2018).
18. D. Szklarczyk, R. Kirsch, M. Koutrouli, K. Nastou, F. Mehryary, R. Hachilif, A. L. Gable, T. Fang, Nadezhda, S. Pyysalo, P. Bork, Lars, Christian, The STRING database in 2023: protein–protein association networks and functional enrichment analyses for any sequenced genome of interest. *Nucleic Acids Research* **51**, D638-D646 (2023).

19. L. Xia, W. Huang, M. Bellani, M. M. Seidman, K. Wu, D. Fan, Y. Nie, Y. Cai, Y. W. Zhang, L.-R. Yu, H. Li, C. A. Zahnow, W. Xie, R.-W. Chiu Yen, F. V. Rassool, S. B. Baylin, CHD4 Has Oncogenic Functions in Initiating and Maintaining Epigenetic Suppression of Multiple Tumor Suppressor Genes. *Cancer Cell* **31**, 653-668.e657 (2017).
20. C. Tabula Muris, c. Overall, c. Logistical, c. Organ, processing, p. Library, sequencing, a. Computational data, a. Cell type, g. Writing, g. Supplemental text writing, i. Principal, Single-cell transcriptomics of 20 mouse organs creates a Tabula Muris. *Nature* **562**, 367-372 (2018).
21. R. K. Davidson, S. A. Weaver, N. Casey, S. Kanojia, E. Hogarth, R. Schneider Aguirre, E. K. Sims, C. Evans-Molina, J. M. Spaeth, The Chd4 subunit of the NuRD complex regulates Pdx1-controlled genes involved in beta-cell function. *J Mol Endocrinol* **69**, 329-341 (2022).
22. R. K. Davidson, S. Kanojia, W. Wu, T. Kono, J. Xu, M. Osmulski, R. N. Bone, N. Casey, C. Evans-Molina, E. K. Sims, J. M. Spaeth, The Chd4 Helicase Regulates Chromatin Accessibility and Gene Expression Critical for beta-Cell Function In Vivo. *Diabetes* **72**, 746-757 (2023).
23. S. R. Hingorani, E. F. Petricoin, A. Maitra, V. Rajapakse, C. King, M. A. Jacobetz, S. Ross, T. P. Conrads, T. D. Veenstra, B. A. Hitt, Y. Kawaguchi, D. Johann, L. A. Liotta, H. C. Crawford, M. E. Putt, T. Jacks, C. V. E. Wright, R. H. Hruban, A. M. Lowy, D. A. Tuveson, Preinvasive and invasive ductal pancreatic cancer and its early detection in the mouse. *Cancer Cell* **4**, 437-450 (2003).
24. B. Thorens, D. Tarussio, M. A. Maestro, M. Rovira, E. Heikkila, J. Ferrer, Ins1(Cre) knock-in mice for beta cell-specific gene recombination. *Diabetologia* **58**, 558-565 (2015).
25. U. Ahlgren, J. Jonsson, L. Jonsson, K. Simu, H. Edlund, beta-cell-specific inactivation of the mouse Ipf1/Pdx1 gene results in loss of the beta-cell phenotype and maturity onset diabetes. *Genes Dev* **12**, 1763-1768 (1998).
26. M. Gannon, E. T. Ables, L. Crawford, D. Lowe, M. F. Offield, M. A. Magnuson, C. V. Wright, pdx-1 function is specifically required in embryonic beta cells to generate appropriate numbers of endocrine cell types and maintain glucose homeostasis. *Dev Biol* **314**, 406-417 (2008).
27. D. F. Boyer, Y. Fujitani, M. Gannon, A. C. Powers, R. W. Stein, C. V. Wright, Complementation rescue of Pdx1 null phenotype demonstrates distinct roles of proximal and distal cis-regulatory sequences in pancreatic and duodenal expression. *Dev Biol* **298**, 616-631 (2006).
28. A. Marciniak, C. M. Cohrs, V. Tsata, J. A. Chouinard, C. Selck, J. Stertmann, S. Reichelt, T. Rose, F. Ehehalt, J. Weitz, M. Solimena, M. Slak Rupnik, S. Speier, Using pancreas tissue slices for in situ studies of islet of Langerhans and acinar cell biology. *Nat Protoc* **9**, 2809-2822 (2014).
29. C. Talchai, S. Xuan, T. Kitamura, R. A. DePinho, D. Accili, Generation of functional insulin-producing cells in the gut by Foxo1 ablation. *Nat Genet* **44**, 406-412, S401 (2012).
30. M. T. Adams, J. M. Dwulet, J. K. Briggs, C. A. Reissaus, E. Jin, J. M. Szulczewski, M. R. Lyman, S. M. Sdao, V. Kravets, S. D. Nimkulrat, S. M. Ponik, M. J. Merrins, R. G. Mirmira, A. K. Linnemann, R. K. Benninger, B. Blum, Reduced synchroneity of intra-islet Ca(2+) oscillations in vivo in Robo-deficient beta cells. *Elife* **10** (2021).
31. M. T. Adams, B. J. Waters, S. D. Nimkulrat, B. Blum, Disrupted glucose homeostasis and glucagon and insulin secretion defects in Robo betaKO mice. *FASEB J* **37**, e23106 (2023).
32. B. J. Waters, Z. R. Birman, M. R. Wagner, J. Lemanski, B. Blum, Islet architecture in adult mice is actively maintained by Robo2 expression in beta cells. *Dev Biol* **505**, 122-129 (2024).
33. M. T. Adams, J. M. Gilbert, J. Hinojosa Paiz, F. M. Bowman, B. Blum, Endocrine cell type sorting and mature architecture in the islets of Langerhans require expression of Roundabout receptors in beta cells. *Sci Rep* **8**, 10876 (2018).

34. J. C. Raum, K. Gerrish, I. Artner, E. Henderson, M. Guo, L. Sussel, J. C. Schisler, C. B. Newgard, R. Stein, FoxA2, Nkx2.2, and PDX-1 Regulate Islet β-Cell-Specific mafA Expression through Conserved Sequences Located between Base Pairs −8118 and −7750 Upstream from the Transcription Start Site. *Molecular and Cellular Biology* **26**, 5735-5743 (2006).
35. M. Perelis, B. Marcheva, K. Moynihan Ramsey, M. J. Schipma, A. L. Hutchison, A. Taguchi, C. B. Peek, H. Hong, W. Huang, C. Omura, A. L. Allred, C. A. Bradfield, A. R. Dinner, G. D. Barish, J. Bass, Pancreatic β cell enhancers regulate rhythmic transcription of genes controlling insulin secretion. *Science* **350**, aac4250-aac4250 (2015).
36. M. Pasdar, Z. Li, V. Chlumecky, Plakoglobin: kinetics of synthesis, phosphorylation, stability, and interactions with desmoglein and E-cadherin. *Cell Motil Cytoskeleton* **32**, 258-272 (1995).
37. J. E. Lewis, J. K. Wahl, K. M. Sass, P. J. Jensen, K. R. Johnson, M. J. Wheelock, Cross-Talk between Adherens Junctions and Desmosomes Depends on Plakoglobin. *The Journal of Cell Biology* **136**, 919-934 (1997).
38. A. P. Kowalczyk, K. J. Green, "Structure, Function, and Regulation of Desmosomes". (Elsevier, 2013), 10.1016/b978-0-12-394311-8.00005-4, pp. 95-118.
39. H. Nguyen, I. W. Glaaser, P. A. Slesinger, Direct modulation of G protein-gated inwardly rectifying potassium (GIRK) channels. *Frontiers in Physiology* **15** (2024).
40. Z. L. Robbe, W. Shi, L. K. Wasson, A. P. Scialdone, C. M. Wilczewski, X. Sheng, A. J. Hepperla, B. N. Akerberg, W. T. Pu, I. M. Cristea, I. J. Davis, F. L. Conlon, CHD4 is recruited by GATA4 and NKX2-5 to repress noncardiac gene programs in the developing heart. *Genes Dev* **36**, 468-482 (2022).
41. J. Miyazaki, K. Araki, E. Yamato, H. Ikegami, T. Asano, Y. Shibasaki, Y. Oka, K. Yamamura, Establishment of a pancreatic beta cell line that retains glucose-inducible insulin secretion: special reference to expression of glucose transporter isoforms. *Endocrinology* **127**, 126-132 (1990).
42. R. Reisdorph, B. Littrell-Miller, R. Powell, N. Reisdorph, A mass spectrometry based predictive strategy reveals ADAP1 is phosphorylated at tyrosine 364. *Rapid Commun Mass Spectrom* **32**, 1173-1180 (2018).
43. A. Shevchenko, H. Tomas, J. Havlis, J. V. Olsen, M. Mann, In-gel digestion for mass spectrometric characterization of proteins and proteomes. *Nat Protoc* **1**, 2856-2860 (2006).
44. H. R. Ali, M. A. Assiri, P. S. Harris, C. R. Michel, Y. Yun, J. O. Marentette, F. K. Huynh, D. J. Orlicky, C. T. Shearn, L. M. Saba, R. Reisdorph, N. Reisdorph, M. D. Hirschey, K. S. Fritz, Quantifying Competition among Mitochondrial Protein Acylation Events Induced by Ethanol Metabolism. *J Proteome Res* **18**, 1513-1531 (2019).
45. J. L. Everman, S. P. Sajuthi, M. A. Liegeois, N. D. Jackson, E. H. Collet, M. C. Peters, M. Chioccioli, C. M. Moore, B. B. Patel, N. Dyjack, R. Powell, C. Rios, M. T. Montgomery, C. Eng, J. R. Elhawary, A. C. Y. Mak, D. Hu, S. Huntsman, S. Salazar, L. Feriani, A. Fairbanks-Mahnke, G. L. Zinnen, C. R. Michel, J. Gomez, X. Zhang, V. Medina, H. W. Chu, P. Cicuta, E. D. Gordon, P. Zeitlin, V. E. Ortega, N. Reisdorph, E. M. Dunican, M. Tang, B. M. Elicker, T. S. Henry, E. R. Bleecker, M. Castro, S. C. Erzurum, E. Israel, B. D. Levy, D. T. Mauger, D. A. Meyers, K. Sumino, D. S. Gierada, A. T. Hastie, W. C. Moore, L. C. Denlinger, N. N. Jarjour, M. L. Schiebler, S. E. Wenzel, P. G. Woodruff, J. Rodriguez-Santana, C. G. Pearson, E. G. Burchard, J. V. Fahy, M. A. Seibold, A common polymorphism in the Intelectin-1 gene influences mucus plugging in severe asthma. *Nat Commun* **15**, 3900 (2024).
46. S. Andrews, FastQC: A Quality Control Tool for High Throughput Sequence Data. (2010).
47. M. Martin, Cutadapt Removes Adapter Sequences From High-Throughput Sequencing Reads. *EMBnet Journal* **17**, 10-12 (2011).

48. A. Dobin, C. A. Davis, F. Schlesinger, J. Drenkow, C. Zaleski, S. Jha, P. Batut, M. Chaisson, T. R. Gingeras, STAR: ultrafast universal RNA-seq aligner. *Bioinformatics* **29**, 15-21 (2013).
49. Y. Liao, G. K. Smyth, W. Shi, featureCounts: an efficient general purpose program for assigning sequence reads to genomic features. *Bioinformatics* **30**, 923-930 (2014).
50. M. I. Love, W. Huber, S. Anders, Moderated estimation of fold change and dispersion for RNA-seq data with DESeq2. *Genome Biol* **15**, 550 (2014).
51. B. Langmead, S. L. Salzberg, Fast gapped-read alignment with Bowtie 2. *Nat Methods* **9**, 357-359 (2012).
52. H. Li, B. Handsaker, A. Wysoker, T. Fennell, J. Ruan, N. Homer, G. Marth, G. Abecasis, R. Durbin, S. Genome Project Data Processing, The Sequence Alignment/Map format and SAMtools. *Bioinformatics* **25**, 2078-2079 (2009).
53. J. Ou, H. Liu, J. Yu, M. A. Kelliher, L. H. Castilla, N. D. Lawson, L. J. Zhu, ATACseqQC: a Bioconductor package for post-alignment quality assessment of ATAC-seq data. *BMC Genomics* **19**, 169 (2018).
54. Y. Zhang, T. Liu, C. A. Meyer, J. Eeckhoute, D. S. Johnson, B. E. Bernstein, C. Nusbaum, R. M. Myers, M. Brown, W. Li, X. S. Liu, Model-based analysis of ChIP-Seq (MACS). *Genome Biol* **9**, R137 (2008).
55. B. G. Stark R, DiffBind: differential binding analysis of ChIP-Seq peak data. . (2011).

**Acknowledgments**

We thank the Sussel lab for providing feedback about experimental design and concepts. A special thank you to Drs. David Lorberbaum and Fiona Docherty for critically reading the manuscript and providing feedback. We also acknowledge Scott K. Beard from the Islet Isolation Core Facility, Barbara Davis Center for his specialty in isolating islets.

**Funding:**

This project was supported by funding from the National Institutes of Health, National Institute of Diabetes and Digestive and Kidney Diseases (NIDDK): Grants R01DK082590 (LS); R01DK106412 (RKPB); R01DK102950 (RKPB); R01DK140904 (RKPB); T32GM136444 (DKS); F31DK131639 (DKS) and the University of Colorado Diabetes Research Center (DRC) P30DK116073.

**Author contributions:**

Conceptualization: DKS, MAG, LS
Methodology: DKS, MAG, LS
Investigation: DKS, TGO, MAG, VMH, CRM
Data Analysis: DKS, CJH, KLW
Supervision: KLW, RKPB, LS
Writing—original draft: DKS, LS
Writing—review & editing: DKS, MAG, VMH, CJH, KLW, RKPB, LS

**Competing interests:**

Authors declare that they have no competing interests.

**Data and materials availability:**

All data needed to evaluate the conclusions in the paper are present in the paper and/or the Supplementary Materials. RNA-sequencing data is available on GEO (GSE299270). ATAC-sequencing was reanalyzed from a previously published study (GSE217444). Code for the analysis of the sequencing data is available on Github

(https://github.com/CUAnschutzBDC/snakemake_pipelines/tree/6ea22de25f49706bb268502bbd894a4a4b7cdb55/RNA_seq, https://github.com/CUAnschutzBDC/snakemake_pipelines/tree/6ea22de25f49706bb268502bbd894a4a4b7cdb55/ATAC_seq) and docker containers for the RNA-seq and ATAC-seq are available on docker hub (RNA-seq docker: https://hub.docker.com/layers/kwellswrasman/rnaseq_general/v1/images/sha256-2536b14130bba19b70f28d23807f127854cd646bbc4bd4028407eeb35ffea45f, https://hub.docker.com/layers/kwellswrasman/rnaseq_r/v1/images/sha256-36d320d7de293da2a84ff35ab131ef6ebec42ab53934aacc9d4f341f7da33988. ATAC-seq docker: https://hub.docker.com/layers/kwellswrasman/fastq_screen/v1/images/sha256-cf697c13d436f251dc70048adfee58438576698c03e398455c394c2d16ffac59, https://hub.docker.com/layers/kwellswrasman/general_chip/v2/images/sha256-447cd6c6ab57006b75b285f851443b9b9d0bc06c8d882bb1a1cb3387d61cc499, https://hub.docker.com/layers/kwellswrasman/atac_chip_r/v1/images/sha256-e499fc2bcde315a720a442447decb95c3a4fa084466bdf816e164f2e40f01971, https://hub.docker.com/repository/docker/kwellswrasman/picard/tags/v1/sha256-29984d83a5ada3c1799684c36bfb4a1dce6912a105baa3b87828b3ef939ee7de).

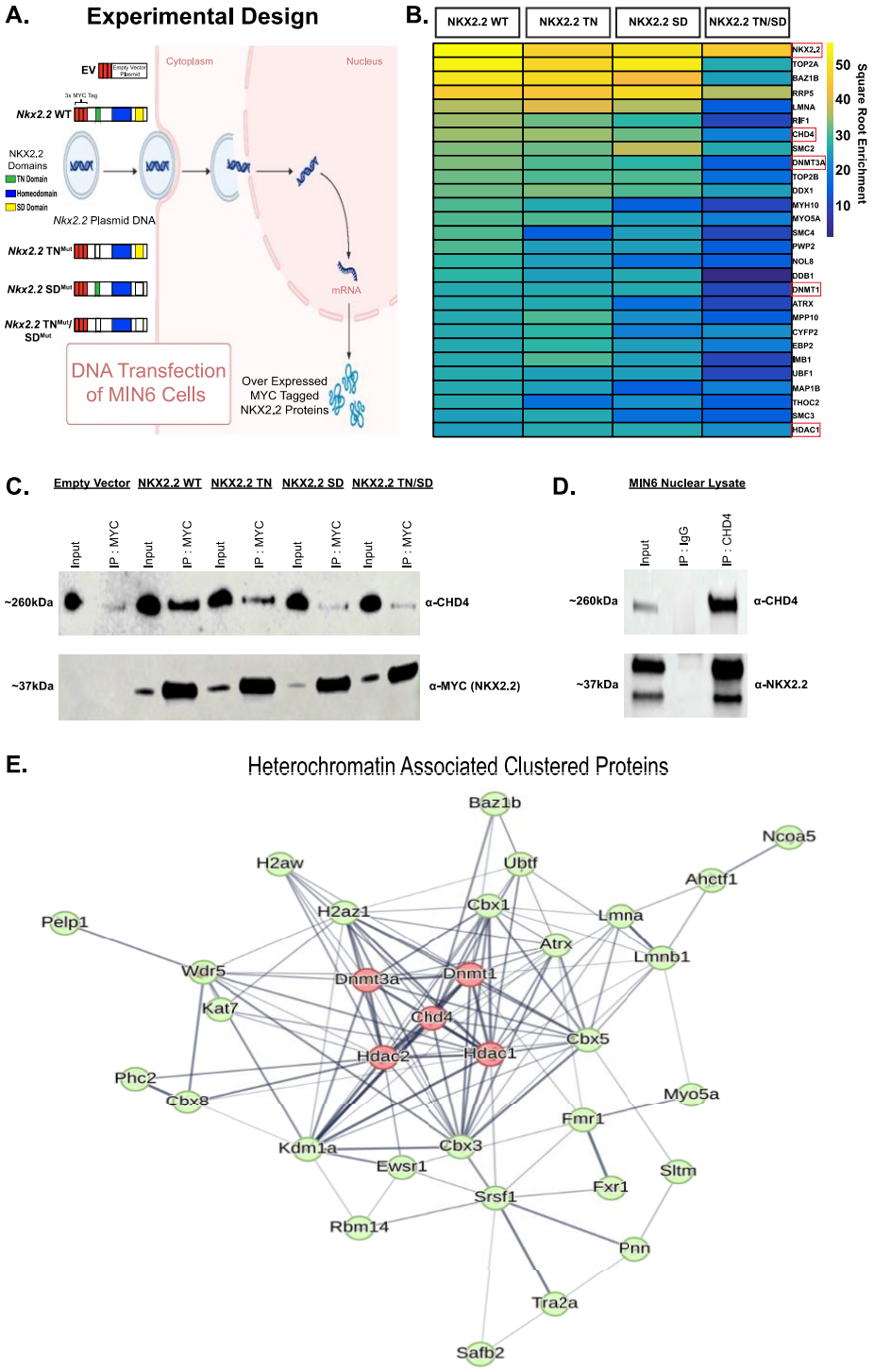


**Fig. 1. NKX2.2 interacts with chromatin modifying protein CHD4.** (A) Schematic for transfection of *Nkx2.2* plasmids with WT and mutant domains into MIN6 β cell culture line for IP-MS. Empty Vector (EV) used as control. (B) Heatmap showing a subset of the highest enriched proteins to come out of the NKX2.2 IP-MS for WT NKX2.2 and each domain mutant. Color represents square root normalization of enrichment. (C) Western blot of MYC tag IP in MIN6 nuclear lysate. (D) Western blot of CHD4 IP in MIN6 nuclear lysate. (E) Heterochromatin group cluster from string database clustering (18) showing overlapping CHD4 and NKX2.2 interacting proteins.

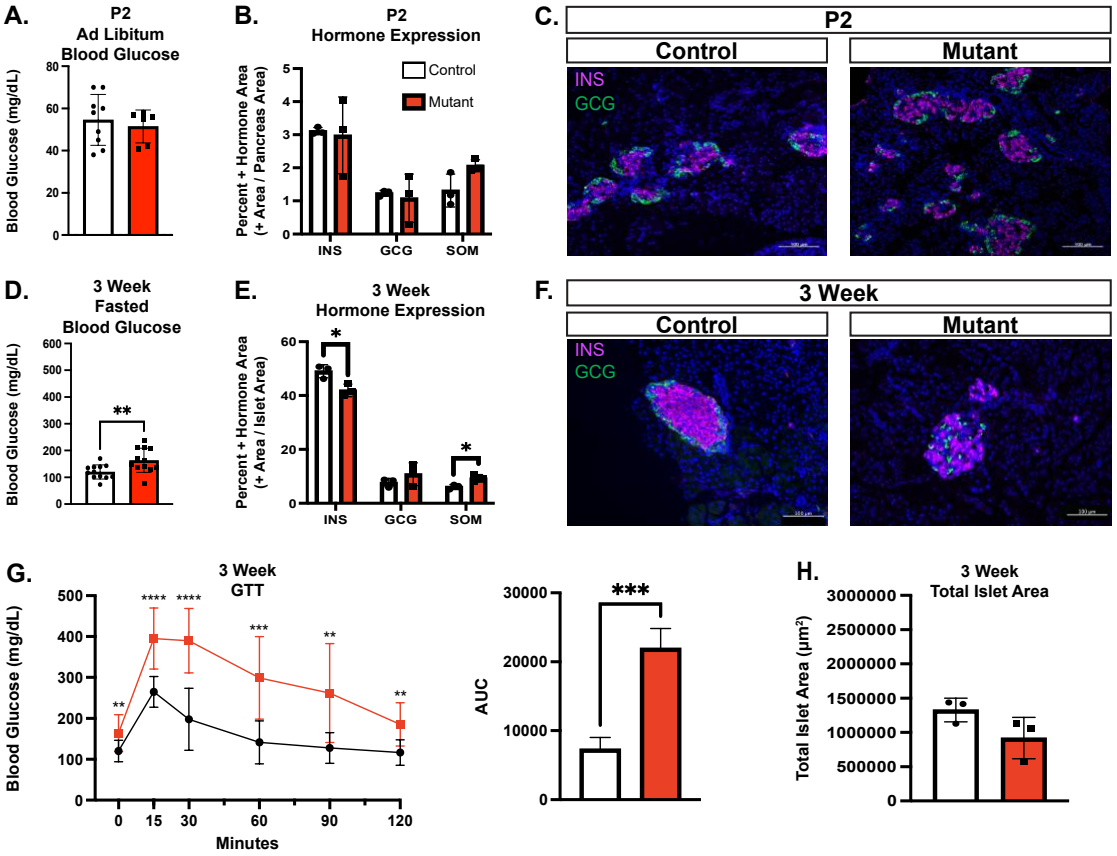


**Fig. 2. *Chd4* βKO mice are hyperglycemic with disrupted islet architecture and dysfunctional β cells.**

Unless otherwise noted, mouse data consists of control (*Chd4*$^{fl/fl}$ : white bars) and mutant/*Chd4* βKO (*Chd4*$^{fl/fl}$*; Ins1*$^{Cre/+}$: red bars) genotypes.

(A) Measurements of *Ad libitum* blood glucose for P2 control (n =6) and mutant (n=9*)* mice. (B) Islet hormone quantification at P2 for Insulin (INS), Glucagon (GCG) and Somatostatin (SOM) for control (n=3) and mutant (n=3) mice. (C) Representative immunofluorescent images for P2 control and mutant mice showing DAPI (blue), Insulin (INS, Magenta), and Glucagon (GCG, green). Scale bars: 100 µm. (D) Measurements of fasted blood glucose for 3-week control (n =12) and mutant (n=12*)* mice. (E) Islet hormone quantification at 3-weeks for Insulin (INS), Glucagon (GCG) and Somatostatin (SOM) for Control (n=3) and Mutant (n=3) mice. (F) Representative immunofluorescent images for 3-week control and mutant mice showing DAPI (blue), Insulin (INS, Magenta), and Glucagon (GCG, green). Scale bars: 100 µm. (G) Glucose Tolerance Test (GTT) of 3-week control (black line, n=12) and mutant (red line, n=12) mice (multiple comparison two-tailed Student's *t*-test). Area under the curve (AUC) measurement for GTT. All points normalized to 0 minutes time point prior to AUC calculation. (H) Quantification of 3-week control (n=3) and mutant (n=3) total islet area. For all figures, *$P \leq 0.05$, **$P \leq 0.01$, ***$P \leq 0.001$, ****$P \leq 0.0001$; two-tailed Student's *t*-test unless otherwise specified.

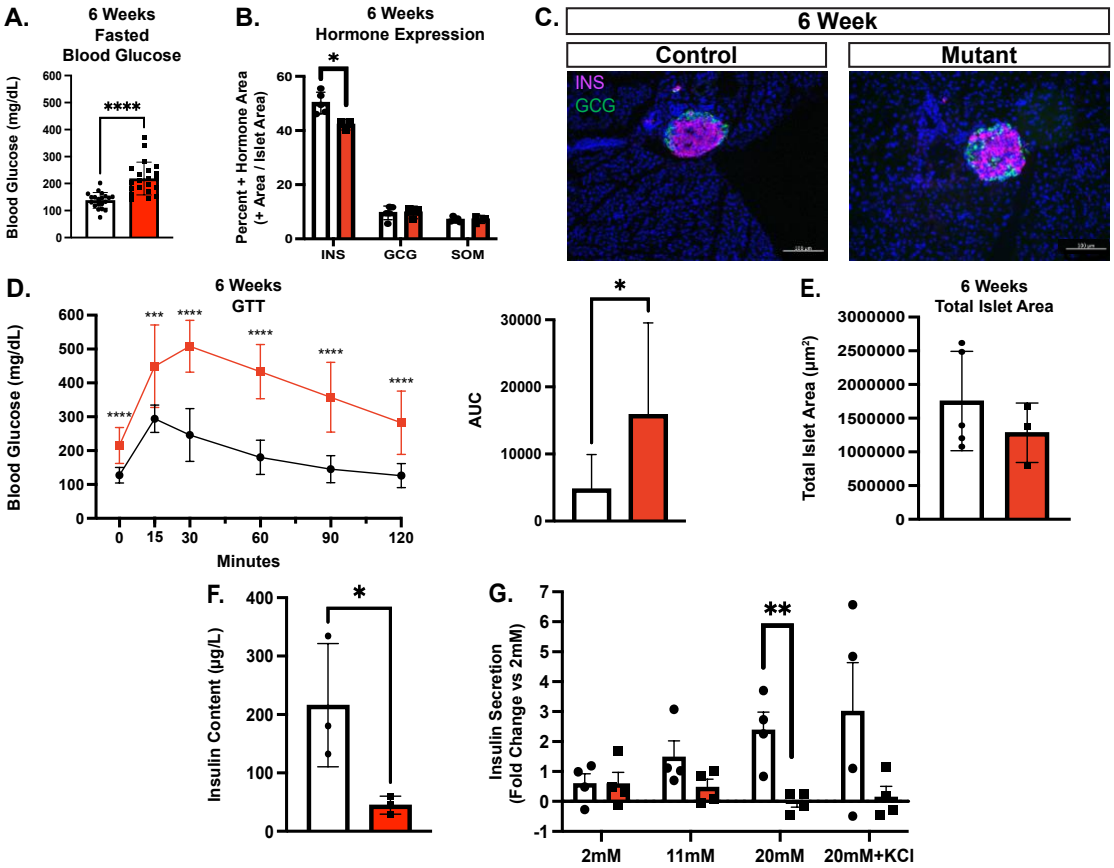


**Fig. 3. *Chd4* βKO mice are hyperglycemic with disrupted islet architecture and dysfunctional β cells.**

Unless otherwise noted, mouse data consists of control (*Chd4*$^{fl/fl}$ : white bars) and mutant/*Chd4* βKO (*Chd4*$^{fl/fl}$*; Ins1*$^{Cre/+}$: red bars) genotypes.
(A) Measurements of fasted blood glucose for 6-week control (n =20) and mutant (n=23*)* mice. (B) Islet hormone quantification at 6-weeks for Insulin (INS), Glucagon (GCG) and Somatostatin (SOM) for control (n=5) and mutant (n=3) mice. (C) Representative immunofluorescent images for 6-week control and mutant mice showing DAPI (blue), Insulin (INS, Magenta), and Glucagon (GCG, green). Scale bars: 100 µm. (D) Glucose Tolerance Test (GTT) of 6-week control (black line, n=13) and mutant (red line, n=13) mice (multiple two-tailed Student's *t*-test). Area under the curve (AUC) measurement for GTT. All points normalized to 0 minutes time point prior to AUC calculation. (E) Quantification of 6-week control (n=5) and mutant (n=3) total islet area. (F) Insulin content from dissected mouse pancreas of 6-week Control (n=3) and Mutant (n=3). (G) Glucose Stimulated Insulin Secretion (GSIS) assay of 6-week control and mutant pancreas slices. Conditions were 2mM glucose, control (n=4) and mutant (n=4), 11mM glucose, Control (n=4) and Mutant (n=4), 20mM glucose, control (n=4) and mutant (n=4), 20mM glucose + KCl, control (n=4) and mutant (n=4). Fold Change is each condition normalized to 2mM basal secretion levels. For all figures, *$P \leq 0.05$, **$P \leq 0.01$, ***$P \leq 0.001$, ****$P \leq 0.0001$; two-tailed Student's *t*-test unless otherwise specified.

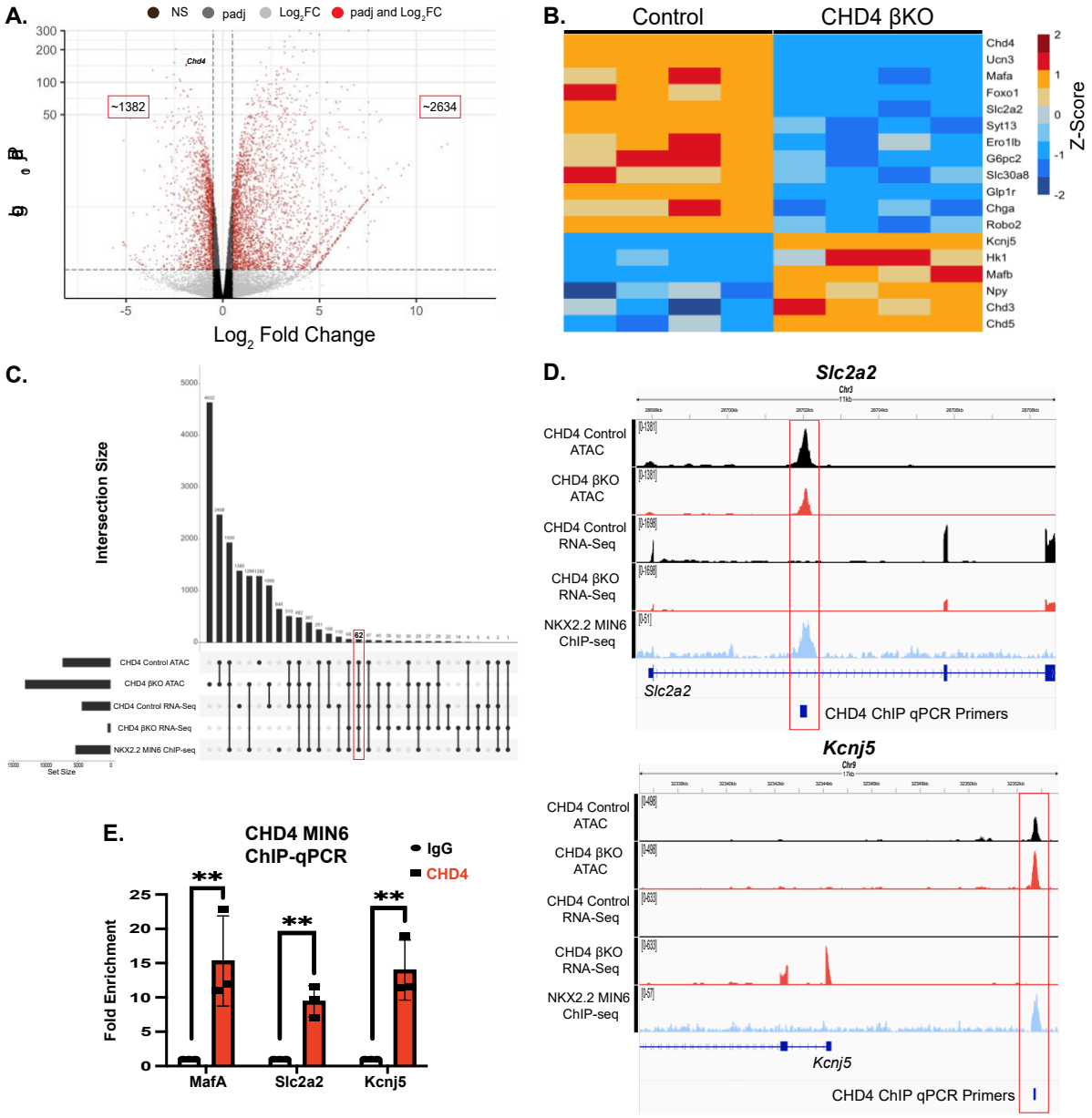


**Fig. 4. CHD4 binds and regulates essential pancreatic β cell genes.**
(A) Volcano plot showing the distribution of differentially expressed genes (DEGs) in *Chd4* βKO mice. (B) Heatmap showing a subset of differentially expressed β cell genes between control and *Chd4* βKO mice. Heat map is mean centered using z-score scale. (C) UpSet plot showing all the genes that overlap in various combinations throughout the five datasets, *Chd4* control and βKO ATAC-seq, *Chd4* and *Nkx2.2* βKO RNA-seq and *Nkx2.2* ChIP-seq datasets. 62 genes overlapped in all five datasets. (D) IGV tracks showing genome locations and sequencing read peaks of *Chd4* control and βKO ATAC-seq, *Chd4* control and βKO RNA-seq and *Nkx2.2* ChIP-seq datasets overlapped with CHD4 binding sites through qPCR primer locations for *Slc2a2* and *Kcnj5.* (E) Quantification of qPCR using fold enrichment over IgG of *MafA, Slc2a2* and *Kcnj5* representing binding sites of CHD4 at these genes (two-tailed Student's *t*-test). $^{**}P \leq 0.01$.

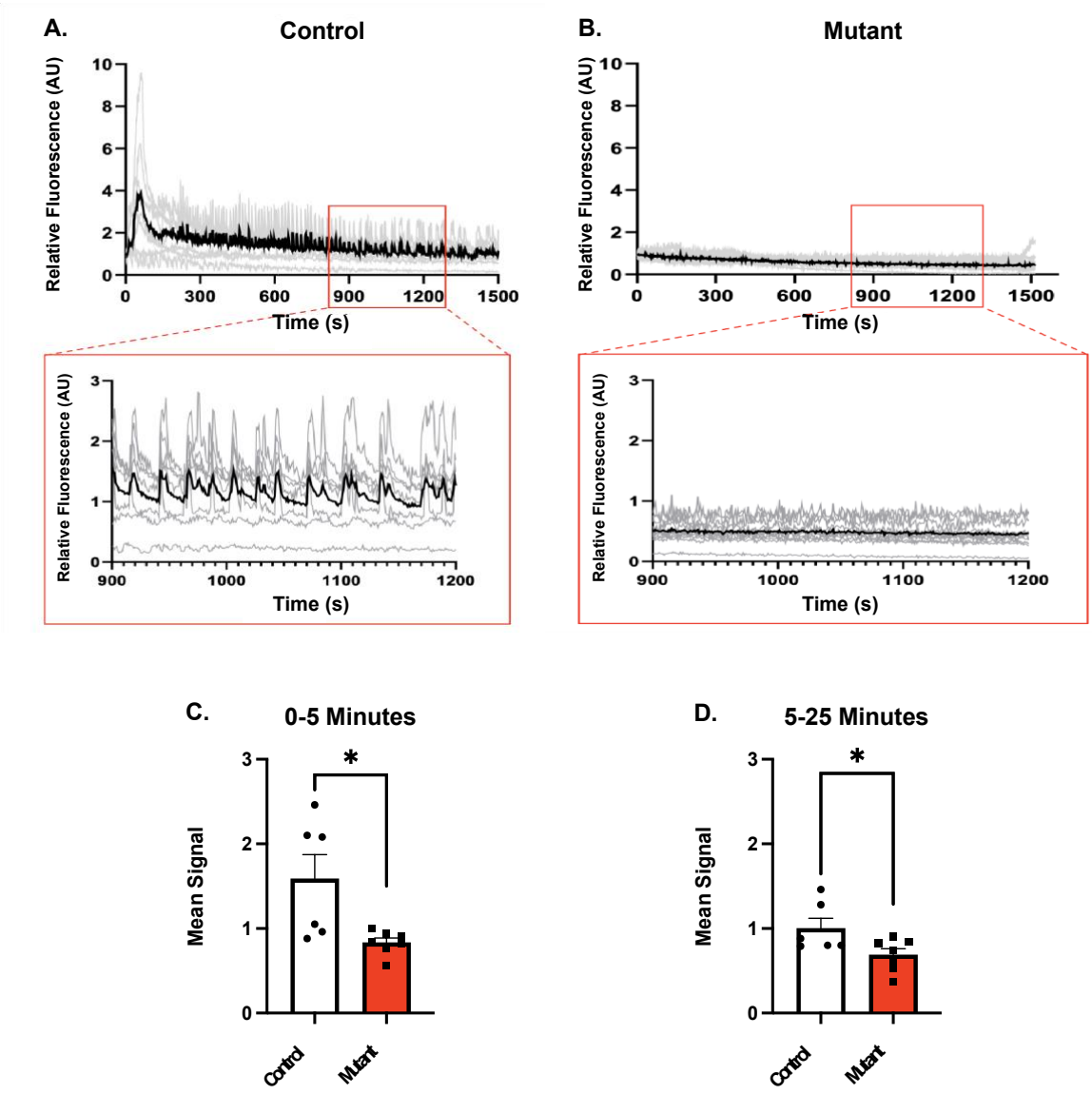


**Fig. 5. Calcium signaling is disrupted in *Chd4* βKO pancreas slice culture.**
(A) Time-course of the Fluo4 $Ca^{2+}$ sensor fluorescence for one islet from a control pancreas slice following elevation of glucose to 11mM. Each gray trace is one cell from the islet, and the black trace is the average fluorescence of all cells from the islet. Fluorescence is normalized to the mean fluorescence at 2mM glucose. Inset box is zoomed in view from 900 to 1200 seconds showing coordinated calcium oscillations in the control islet. (B) Time-course of the Fluo4 $Ca^{2+}$ sensor fluorescence for one islet from mutant pancreas slice, as in A. (C) Quantification of mean Fluo4 signal for the first 5 minutes after $Ca^{2+}$ elevation, for control (n=6) and mutant (n=6) pancreas slices. Mean signal = average fluorescence over indicated time (two-tailed Student's *t*-test). (D) Quantification of mean signal for 5 minutes to 25 minutes after $Ca^{2+}$ elevation for control (n=6) and mutant (n=6) pancreas slices, as in C (two-tailed Student's *t*-test). *$P \leq 0.05$.